Available online at www.sciencedirect.com
ScienceDirect
Trans. Nonferrous Met. Soc. China 27(2017) 977−985
Transactions of Nonferrous Metals Society of China
www.tnmsc.cn

Influence of ultrasonic treatment on formation of primary Al_3Zr in Al−0.4Zr alloy

Feng WANG[1], D. ESKIN[1,2], T. CONNOLLEY[3], Jia-wei MI[4]

1. Brunel Centre for Advanced Solidification Technology, Brunel University London, Uxbridge, London, UB8 3PH, UK;
2. Tomsk State University, Tomsk 634050, Russia;
3. Diamond Light Source Ltd., Harwell Science & Innovation Campus, Didcot, OX11 0DE, UK;
4. School of Engineering, University of Hull, Hull, East Yorkshire, HU6 7RX, UK

Received 29 May 2016; accepted 28 December 2016

Abstract: The effect of ultrasonic treatment on the formation of primary Al_3Zr was investigated by applying ultrasound to an Al−0.4Zr alloy. Three temperature ranges were selected, i.e., 830 to 790 °C (above liquidus), 790 to 750 °C (cross liquidus) and 750 to 710 °C (below liquidus) for ultrasonication. Using the scanning electron microscopy, both the size and morphology of the primary Al_3Zr particles were examined. It was found that the size was significantly reduced and the morphology changed from large throwing-star shape to small compact tablet shape. The mechanisms for refinement of primary Al_3Zr were discussed. It is suggested that sonocrystallization theory via activation of aluminium oxide particles is responsible for the refinement of primary Al_3Zr when ultrasonic melt treatment (UST) is applied within the fully liquid state. The refinement of primary Al_3Zr particles when UST is applied in the slurry (growth stage) is due to the sonofragmentation.
Key words: ultrasonic treatment; aluminium alloy; primary Al_3Zr intermetallic; refinement; crystal morphology

1 Introduction

Primary crystals formed in aluminium alloys play an important role in affecting the properties of castings. Under normal casting conditions, the primary crystals may grow to a considerable size with elongated shape, which makes them stress concentrators and hence origins of cracks as most of the primary crystals are brittle. As a result, the primary particles usually deteriorate the ductility, toughness and deformability of as-cast alloys [1,2]. However, when refined to an appropriate size, the primary particles can serve as reinforcing structure constituent to form natural metal-matrix composites [3]. Hypereutectic Al−Si alloy containing more than 12% Si (mass fraction unless otherwise stated) is one of the best-known examples [3,4]. Homogeneous distribution of fine primary Si particles enables the hypereutectic Al−Si alloy to possess a unique combination of properties, i.e., low coefficient of thermal expansion, high elastic modulus, hardness and wear resistance, good corrosion resistance, weldability and low density. In addition, some of the primary intermetallics [5−7] show a considerable potential as grain refiners for the primary matrix grains. Increasing the number of these promising primary intermetallics by refinement could further promote grain refinement of the alloy matrix and thus enhance the properties of castings. Therefore, significant refinement of the primary crystals that either act as reinforcing particles or grain refiners can essentially improve the structure, properties, and workability of cast alloys.

Ultrasonic melt treatment (UST) is one of the efficient means to refine primary crystals in metallic alloys [4,8,9]. Although the general mechanisms underlying the refining effect of UST have been formulated in Refs. [4,9], the specific mechanisms responsible for the refinement of free-growing primary crystals under different processing conditions are still not well understood. It is recognized [5,9−11] that the efficiency of UST is determined by many factors such as the amplitude and frequency of ultrasound, treatment temperature and duration, and the solidification conditions including cooling rate, alloy composition and

Corresponding author: Feng WANG; E-mail: feng.wang@brunel.ac.uk
DOI: 10.1016/S1003-6326(17)60115-8

impurity level. Among all these factors, the treatment temperature range is considered to be of critical importance. It is fundamental knowledge [1,2] that different temperature ranges for alloys with different compositions correspond to different solidification stages, i.e., nucleation and growth. Therefore, UST over different temperature ranges may involve different mechanisms which essentially control the effect of UST.

ATAMANENKO et al [5] and ZHANG et al [11] observed the refinement of primary Al(Zr, Ti)$_3$ particles after applying UST in an Al−Zr−Ti alloy though their major focus was on the refinement of α(Al) grains. In this work, a follow-up work on the influence of UST on the formation of primary Al_3Zr particles in an Al−0.4%Zr alloy was presented. UST was applied over three different temperature ranges to clarify the role of UST at different solidification stages. Furthermore, the possible mechanisms that control the effect of UST were discussed based on the theories proposed in the literature.

2 Experimental

2.1 Materials and equipment

High-purity commercial aluminium (99.97%) and an Al−10%Zr master alloy were used to prepare an Al−0.4%Zr alloy. The liquidus temperature of primary Al_3Zr in the Al−0.4%Zr alloy was calculated to be 788 °C using Thermo Calc software [12].

The ultrasonic device consisted of a 5 kW ultrasonic generator, a magnetostrictive transducer with water cooling system and a conical niobium sonotrode. Ultrasonic treatment was performed at 4 kW power and a frequency of 17.5 kHz and a corresponding null-to-peak amplitude of 40 μm.

2.2 Experiment procedure

Pure Al (~750 g for each experiment) was melted and heated up to (880±3) °C in a clay-bonded graphite crucible inside an electrical resistance furnace. After adding the master alloy, the melt was isothermally held at 880 °C for 20 min to allow the complete dissolution of the master alloy. Following that, a sample for composition analysis was cast into a steel mould that was preheated at 200 °C and the crucible with the remaining melt was transferred to a platform where the ultrasound was applied to the melt. The melt was then cooled down in air, and its temperature was monitored by a K-type thermocouple positioned at approximately half the radius away from the wall of crucible. When the melt cooled down to the commencement temperature of UST, the vibrating sonotrode was immersed 15 mm below the top surface of the melt. Considering the chill effect of a cold sonotrode, the working sonotrode was preliminary preheated inside a large mass (~2.5 kg) of pure Al melt (~850 °C) for about 30 s before it was inserted into the melt to be treated. This operation minimized the temperature drop upon the immersion of the sonotrode in the melt, and therefore the cooling rate change was negligible. For comparison, a parallel experiment without UST was also carried out by immersing the idle sonotrode (without being switched on) into the melt at the same temperature as the experiment with UST. The sonotrode was not lifted up from the melt until the melt temperature reached the designed termination temperature of UST. The melt together with the crucible was then left on the platform to solidify in air to room temperature. The overall cooling rate measured by thermocouple was ~0.8 °C/s. Three temperature ranges were selected, corresponding to three different solidification stages: 830 to 790 °C (fully liquid state), 790 to 750 °C (the nucleation stage of primary Al_3Zr), and 750 to 710 °C (the growth stage of primary Al_3Zr). The chemical compositions of the alloys were analyzed by inductively coupled plasma-atomic emission spectroscopy (ICP-AES) and the averaged values are listed in Table 1.

Table 1 Average values of chemical compositions of Al−0.4% Zr alloys

Zr	Ti	B
0.40±0.02	0.008±0.001	0.0025±0.0008
Si	Fe	Al
0.03±0.005	0.09±0.001	Bal.

2.3 Sample preparation and examination

The ingots solidified in the crucible were longitudinally sectioned along the centre symmetrical axis and specimens were prepared from the central bottom part as shown in the schematic diagram (Fig. 1), because most of the primary Al_3Zr particles settled down to the ingot bottom during the solidification due to the

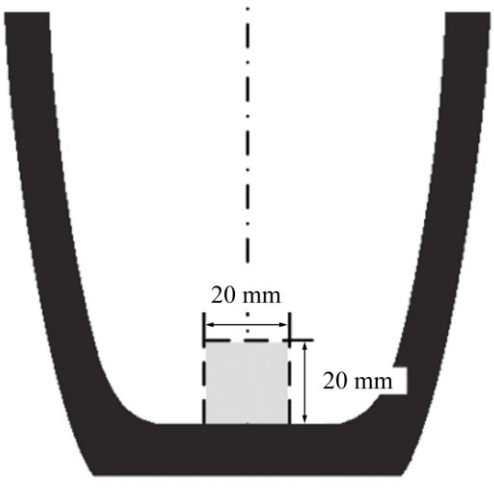

Fig. 1 Schematic diagram of relative position of specimen

large density of Al_3Zr and slow cooling rate. The specimens were then mechanically ground and polished for X-ray diffraction analysis (XRD, Bruker D8 Advance diffractometer) and scanning electron microscopy (SEM, Zeiss Supra 35VP). Energy dispersive X-ray spectroscopy (EDS) was used to determine the composition of the particles observed in the samples. In order to display the 3D morphology of the primary Al_3Zr intermetallic, the samples with and without UST were deeply-etched by 15% NaOH water solution for about 2 h. The deeply-etched samples were then also examined by SEM.

3 Results and discussion

3.1 Confirmation of identity of primary Al_3Zr intermetallic particles

Normally, under slow cooling rates with and without UST which was the case in the current experiment, the stable tetragonal Al_3Zr phase forms as primary intermetallic particles in the Al−0.4%Zr alloy according to the equilibrium phase diagram [13]. However, it was also reported that under certain solidification conditions such as fast cooling rate, the formation of stable Al_3Zr might be suppressed or even the metastable Al_3Zr phase with a cubic crystal structure may be formed [14,15]. In order to ascertain the formation of the stable tetragonal Al_3Zr phase, the samples with and without UST were examined by XRD and SEM−EDS. Figure 2 shows the typical XRD spectrum and EDS spectra of the particles observed in the backscattered electron (BSE) images of the Al−0.4% Zr alloys with and without UST. As we can see, the XRD spectrum in Fig. 2(a) presents only reflection peaks from Al and tetragonal Al_3Zr phases. In addition, the EDS spectra in Figs. 2(d) and (e) obtained for the particles

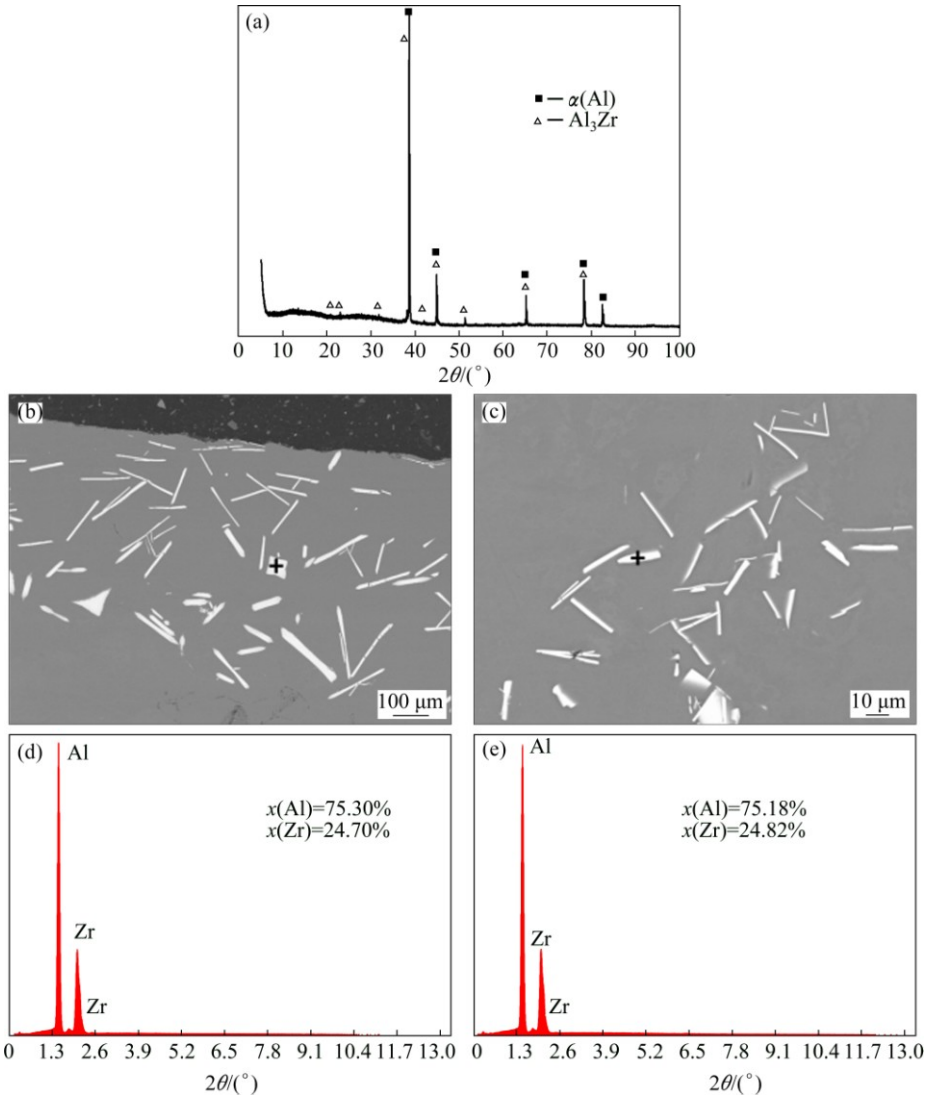

Fig. 2 Typical XRD spectrum of Al−0.4%Zr alloys produced with and without UST (a), typical SEM-BSE images of Al−0.4%Zr alloy without UST (b) and with UST (c), EDS spectra of particles observed in SEM−BSE image of Al−0.4%Zr alloy without UST (d) and with UST (e)

shown in Figs. 2(b) and (c) indicate that the particles are high in Al and Zr with the mole ratio close to 75:25. Combining the XRD and EDS spectra analysis, we can conclude that the Al−0.4% Zr alloys produced with and without UST consist of only Al and primary tetragonal Al_3Zr phases.

3.2 Effect of UST on size of primary Al_3Zr intermetallic particles

Typical SEM−BSE images of primary Al_3Zr intermetallic particles in the Al−0.4% Zr alloys solidified without and with UST performed over the three selected temperature ranges are given in Fig. 3. It is clear that UST over all the tested temperature ranges produced considerable refinement of primary Al_3Zr particles. Figure 4 shows the measured size distributions of primary Al_3Zr particles in the samples. As we can see in Figs. 3(a) and 4, primary Al_3Zr particles in the samples solidified without UST have relatively large size with majority of them in the range of 50−150 μm and some of the particles even reaching 350 μm. This is easy to understand considering the large solidification range (~127 °C with 0.4% Zr in Al) of primary Al_3Zr and the slow cooling rate (~0.8 °C/s) which allows sufficient time for the primary Al_3Zr particles to grow. From Figs. 3(b) and 4(a) we can see that the majority of the primary particles are well refined to the range of 25−75 μm with the maximum size reaching only 150 μm after UST was applied above the liquidus of intermetallics. Figures 3(c) and 4(b) show that UST performed from 790 to 750 °C (across the liquidus) refines the majority of the particles to 15−50 μm. The

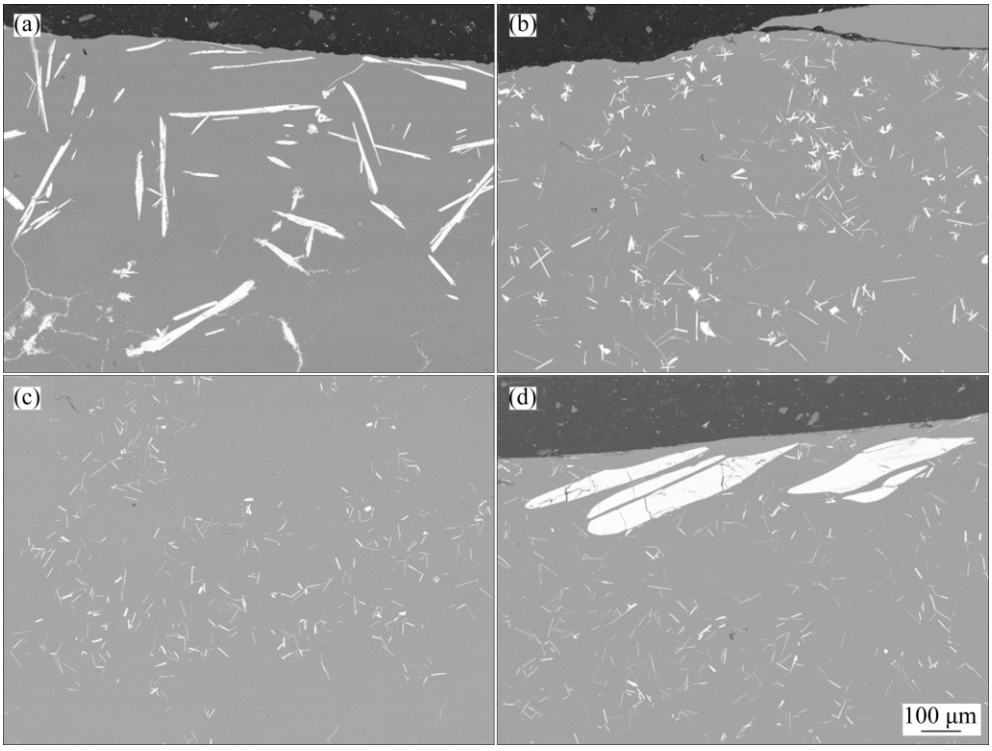

Fig. 3 Typical SEM−BSE micrographs of primary Al_3Zr intermetallic particles form samples obtained without UST (a), with UST performed at 830−790 °C (b), with UST performed at 790−750 °C (c), and with UST performed at 750−710 °C (d)

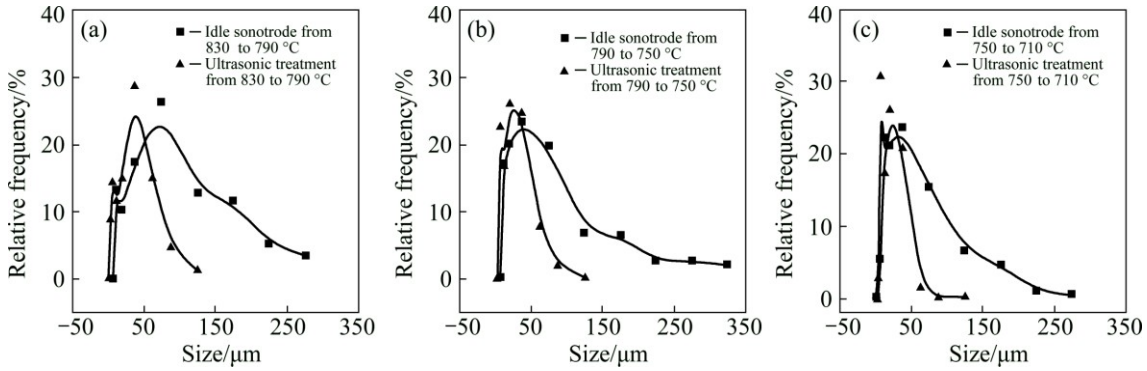

Fig. 4 Size distribution of primary Al_3Zr particles in samples obtained with UST at 830−790 °C (a), 790−750 °C (b), 750−710 °C (c) in comparison with samples obtained without UST under similar conditions (idle sonotrode)

size distribution of primary particles after the UST from 750 to 710 °C is illustrated in Fig. 4(c) with corresponding structure in Fig. 3(d). As we can see, the majority of the particles are refined to 25−75 μm. However, some particles have as large size as 300 μm.

It is interesting to point out that in the present work UST within the fully liquid state from 830 to 790 °C (while the liquidus temperature of primary Al_3Zr is 788 °C) induced remarkable refinement of primary Al_3Zr particles as shown in Figs. 3(b) and 4(a). On the other hand, when UST is performed only in the slurry region from 750 to 710 °C, in addition to small particles, there are some very large particles as shown in Figs. 3(d) and 4(c).

3.3 Effect of UST on 3D morphology of primary Al_3Zr intermetallic particles

Figure 5 shows the typical SEM images of the 3D morphology of primary Al_3Zr particles after deep etching of the samples without UST. As we can see in Fig. 5(a), almost all the primary Al_3Zr particles have a thin plate shape with four obvious apexes. This shape is quite like one of the ancient Chinese weapons: the throwing stars. The evident faceted morphology of the primary Al_3Zr particles can be readily explained in terms of the well-established growth behaviour of crystals in melt. It is known [1,2] that ordered intermetallic compounds that often have high entropy of fusion due to the great difference in structure and bonding between the solid and liquid phases usually show a high growth rate anisotropy which leads to the development of a faceted morphology.

Furthermore, the specific faceted morphology of a crystal is closely related to its crystal structure [16]. In the case of the tetragonal Al_3Zr phase, the broad plane belongs to the {001} plane family while the four apexes are the fast growing ⟨110⟩ directions as indicated in Figs. 5(b) and (c) [17,18]. The essentially two-dimensional growth of primary Al_3Zr particles is because the growth rate of {001} planes is considerably lower than that of other crystallographic planes due to the high crystalline perfection of the {001} planes at the atomic scale which makes it too difficult for atoms to attach to these planes [16,19]. In addition, the development of the four apexes at corners and of the concave points at edge centres is because the rate of nucleation of new ledges at corners is significantly higher than the rate of propagation of the ledges across the edges. This is a consequence of a locally thinner Zr-solute depleted layer ahead of the interface at the corners than at the edge centres, which results in higher gradients of constitutional undercooling at the corners than at the edge centres [20].

In addition to the common “throwing-star” morphology, some interesting morphologies in Fig. 5(d) have been observed. As we can see, a few primary Al_3Zr particles are intersecting each other, forming a petal-like morphology. This is possibly because these particles have grown from a twinned nucleation centre that has several twins [21].

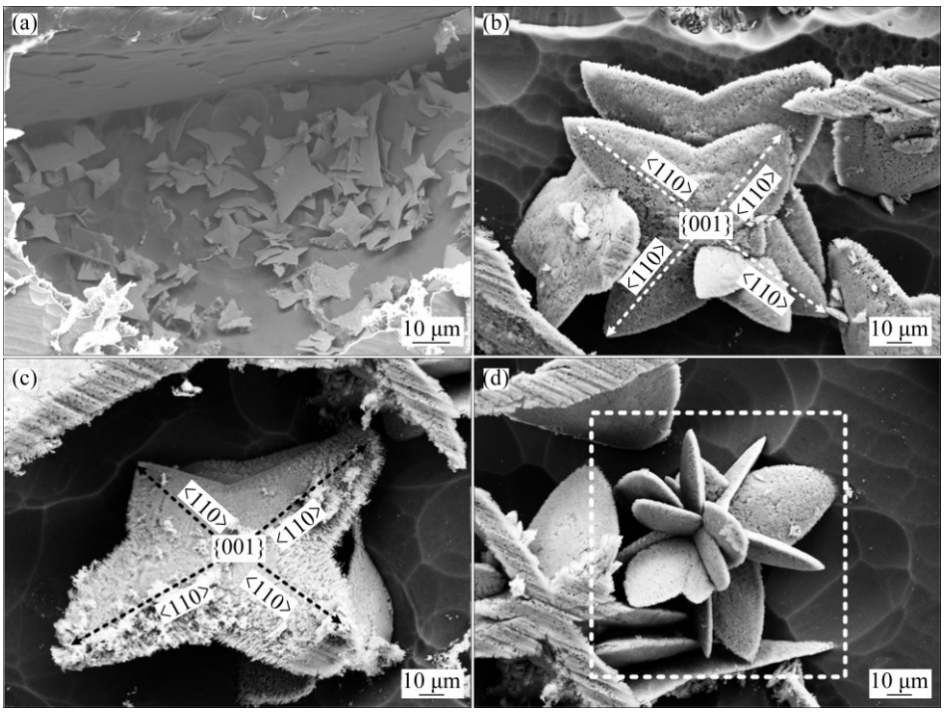

Fig. 5 Typical SEM images of primary Al_3Zr particles after deep etching of samples without UST: (a) Large number of Al_3Zr particles with typical morphology; (b, c) Two particular Al_3Zr particles showing four preferential growth directions; (d) Special Al_3Zr particle with petal morphology

Figure 6 shows the typical morphology of primary Al_3Zr particles after UST over all the three selected temperature ranges. Apparently, the particles are still plate-like in shape only with a smaller size and thickness since they are refined as a result of UST. The very obvious difference from the morphology of non-refined particles is that there are no well-developed apexes at corners and no concave points at edge centres. Instead, the refined particles exhibit nearly perfect tablet morphology. From the schematic diagram of the growth mechanism of faceted dendrites [20,22] as shown in Fig. 7, we can see that the refined primary Al_3Zr particles display the morphology at stage (1) while the non-refined primary Al_3Zr particles exhibit the morphology at stage (2). It is hence understandable that, due to the refining effect induced by UST, the primary Al_3Zr particles can only grow to a limited size, not reaching conditions for the perturbations to develop.

3.4 Mechanisms of UST refinement over selected temperature ranges

In order to understand the refining mechanisms of UST over the three selected temperature ranges, the results of present study are discussed in light of the theories available in literatures.

The influence of UST on the microstructure changes including refinement of grains and primary particles is mainly due to the physical phenomena that arise from the propagation of the high intensity ultrasound through the liquid [9,23]. Two of the most important phenomena are acoustic cavitation which is the formation, growth and implosive collapse of cavitation bubbles and acoustic streaming which is the formation of a steady flow driven by acoustic wave propagation and cavitation region pulsation. On the basis of these phenomena, a number of hypotheses have been proposed to clarify the chemical and physical effects of ultrasound. In general, these

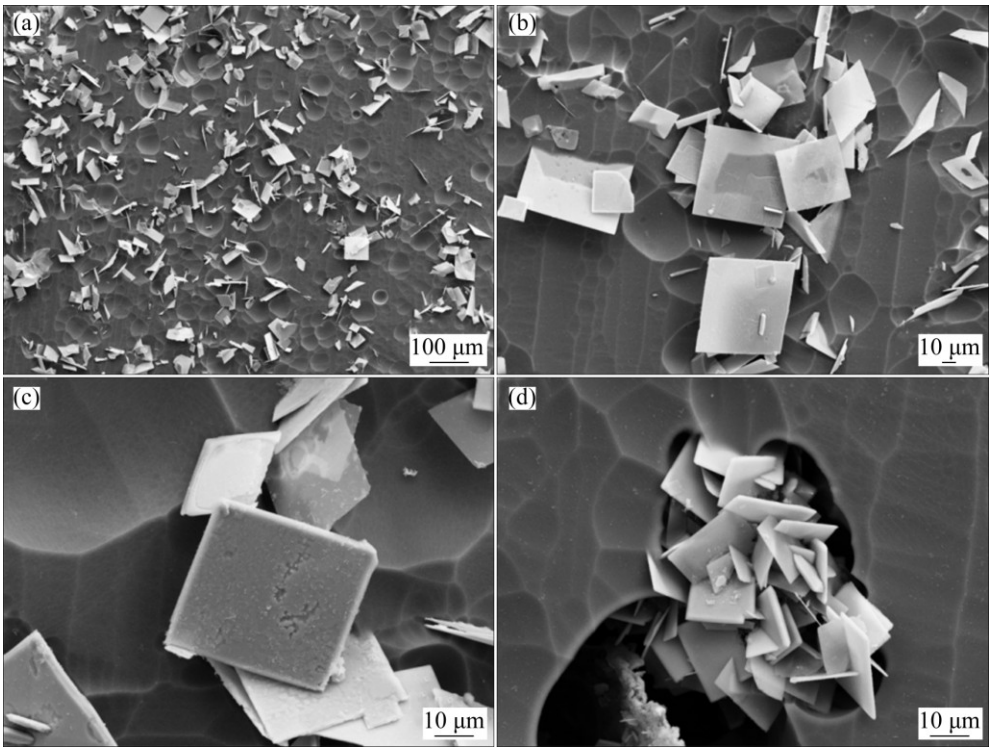

Fig. 6 Typical SEM images of primary Al_3Zr particles after deep etching of samples with UST applied at 790−750 °C (Figures (b), (c) and (d) are selected enlarged images of particles shown in Fig. (a))

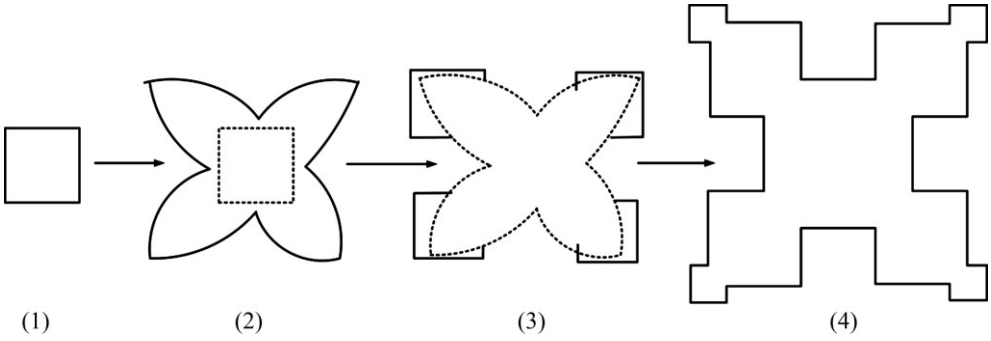

Fig. 7 Schematic diagram showing development of faceted dendrites [20,21]

hypotheses can be summarized as two theories [5,9,10,24,25]: 1) the sonocrystallization theory which is based on cavitation-enhanced nucleation and 2) the sonofragmentation theory which is based on cavitation-induced fragmentation.

Two different mechanisms have been proposed to explain the sonocrystallization theory. The first one [26] suggests that the instantaneous pressure pulse caused by the collapse of cavitation bubbles leads to a local increase in the melting point of the surrounding liquid according to the Clapeyron equation. The increase in the melting point is equivalent to generating locally an increased undercooling which promotes nucleation. The second mechanism [4,9,27] is based on the idea of activation of substrates. Real melt always contains impurity particles which often possess crevices and cracks on their surface and are usually non-wettable by the melt. It is suggested that the formation, growth and implosive collapse of cavitation bubbles close to the micro-crevices or micro-cracks produce a high-energy shockwave or cumulative jet near the impurity particles. Both phenomena would result in the sonocapillary effect that improves wetting of the impurity particles by the melt and hence activates them to become effective nucleation sites.

The sonofragmentation theory [9,10,23,25] assumes that the shockwaves or microjets generated by bubble collapse create shear forces and produce localized erosion on solid phase which leads to the fragmentation of phase. The solid fragments are then distributed throughout the melt via the acoustic streaming and hence increase the number of crystals. It is necessary to emphasize that the sonofragmentation can only happen when a solid phase already exists in the melt and is present in the cavitation zone.

In this study, the application of UST over the temperature range from 830 to 790 °C is most probably related to the sonocrystallization theory since this temperature range is within fully liquid state and no nucleation and growth of the primary Al_3Zr particles is expected to occur. The fact that the primary Al_3Zr particles were refined when UST was applied within the liquid state suggested that the sonocrystallization mechanisms did work above the liquidus temperature. Careful examination of the refined primary Al_3Zr particles after deep etching reveals the presence of foreign particles inside the Al_3Zr particles as shown in Figs. 8(a) and (b). EDS analysis shows that these particles contain O apart from Al and Zr, indicating that this is possibly the aluminium oxide (the Zr peak is due to the pick-up of the surrounding Al_3Zr particle). It has been reported that native oxide particles can act as nucleation sites for Al and Mg grains [28,29] or primary intermetallics [30]. So, the second mechanism of sonocrystallization, i.e., activation of substrates (alumina), is most probably active upon UST above the liquidus temperature of Al_3Zr particles. The authors are now working on the detailed identification and characterization of these potential aluminium oxide particles by transmission electron microscopy and 3D tomography.

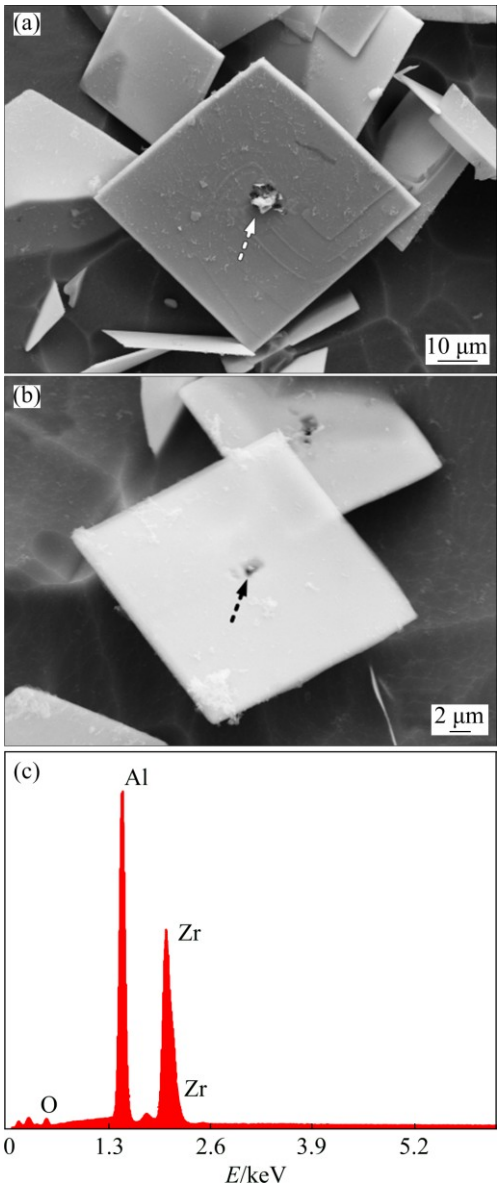

Fig. 8 Foreign particles at centres of primary Al_3Zr particles (a, b) and typical EDS spectrum (c) obtained on foreign particles as indicated in (a) and (b)

On the other hand, UST over the temperature ranging from 750 to 710 °C can be mainly correlated to the sonofragmentation theory because this temperature range generally corresponds to the growth stage of primary Al_3Zr particles, which are expected to already grow to certain sizes since the temperature is well below the liquidus temperature. The co-existence of large and

small primary particles as shown in Fig. 3(d) can be explained as follows: most of the well-grown particles were fragmented by the cavitation-induced shockwaves or microjets while some of them were outside the cavitation zone and continued to grow to a large size. It is worth noting that the authors are currently also working on the in-situ observations of the fragmentation process during UST both in real Al−0.4%Zr alloys using high-energy X-ray synchrotron imaging and in water by high-speed camera.

As to the UST applied from 790 to 750 °C in the present study, considering that both nucleation and growth of primary Al_3Zr particles will occur within this temperature range, it can be argued that both the sonocrystallization and sonofragmentation could have contributed to the observed refinement of primary Al_3Zr particles, similar to the observed recently grain refinement of Al grains when UST is applied across the liquidus temperature [25].

4 Conclusions

1) Considerable refinement of primary Al_3Zr particles is observed as a result of UST over all the three selected temperature ranges. In addition, the morphology is also changed from a “throwing-star” shape to a nearly perfect tablet shape.

2) Sonocrystallization theory via activation of aluminium oxide particles is suggested to be responsible for the refinement of primary Al_3Zr when UST is applied in the fully liquid state. The refinement of primary Al_3Zr particles when UST is applied in the slurry (growth stage) is due to the sonofragmentation.

3) It is suggested that both mechanisms play major role in the refinement of primary Al_3Zr particles when the UST is applied across the liquidus and terminated at the growth stage.

Acknowledgements

The authors acknowledge the financial support from UK Engineering and Physical Science Research Council (EPSRC) for the Ultra-Cast project (grant EP/L019884/1, EP/L019825/1, EP/L019965/1).

References

[1] KURZ W, FISHER D J. Fundamentals of solidification [M]. Zurich, Switzerland: Trans Tech Publications, 1998.

[2] DANTZIG J A, RAPPAZ M. Solidification [M]. Lausanne: EPFL Press, 2009.

[3] ESKIN G I, ESKIN D G. Production of natural and synthesized aluminum-based composite materials with the aid of ultrasonic (cavitation) treatment of the melt [J]. Ultrason Sonochem, 2003, 10: 297−301.

[4] ESKIN G I, ESKIN D G. Some control mechanisms of spatial solidification in light alloys [J]. Z Metallk, 2004, 95: 682−690.

[5] ATAMANENKO T V, ESKIN D G, ZHANG L, KATGERMAN L. Criteria of grain refinement induced by ultrasonic melt treatment of aluminum alloys containing ZR and Ti [J]. Metall Mater Trans A, 2010, 41: 2056−2066.

[6] LIU Z, QIU D, WANG F, TAYLOR J A, ZHANG M. The grain refining mechanism of cast zinc through silver inoculation [J]. Acta Mater, 2014, 79: 315−326.

[7] WANG F, LIU Z, QIU D, TAYLOR J A, EASTON M A, ZHANG M X. Revisiting the role of peritetics in grain refinement of Al alloys [J]. Acta Mater, 2013, 61: 360−370.

[8] ESKIN G I. Broad prospects for commercial application of the ultrasonic (cavitation) melt treatment of light alloys [J]. Ultrason Sonochem, 2001, 8: 319−325.

[9] ESKIN G I, ESKIN D G. Ultrasonic treatment of light alloy melts [M]. Boca Raton, Florida: CRC Press, 2015.

[10] QIAN M, RAMIREZ A, DAS A. Ultrasonic refinement of magnesium by cavitation: Clarifying the role of wall crystals [J]. J Cryst Growth, 2009, 311: 3708−3715.

[11] ZHANG L, ESKIN D G, KATGERMAN L. Influence of ultrasonic melt treatment on the formation of primary intermetallics and related grain refinement in aluminum alloys [J]. J Mater Sci, 2011, 46: 5252−5259.

[12] ANDERSSON J O, HELANDER T, HÖGLUND L, SHI P, SUNDMAN B. Thermo-Calc & DICTRA, computational tools for materials science [J]. Calphad, 2002, 26: 273−312.

[13] MURRAY J, PERUZZI A, ABRIATA J P. The Al−Zr (aluminum-zirconium) system [J]. Journal of Phase Equilibria, 1992, 13: 277−291.

[14] DESCH P B, SCHWARZ R B, NASH P. Formation of metastable L12 phases in Al3Zr and Al−12.5%X−25%Zr (X=Li, Cr, Fe, Ni, Cu) [J]. Journal of the Less Common Metals, 1991, 168: 69−80.

[15] NES E, BILLDAL H. Non-equilibrium solidification of hyperperitetic Al−Zr alloys [J]. Acta Metall, 1977, 25: 1031−1037.

[16] PRYWER J. Kinetic and geometric determination of the growth morphology of bulk crystals: Recent developments [J]. Prog Cryst Growth Charact Mater, 2005, 50: 1−38.

[17] LI L, ZHANG Y, ESLING C, JIANG H, ZHAO Z, ZUO Y, CUI J. Crystallographic features of the primary Al_3Zr phase in as-cast Al−1.36wt% Zr alloy [J]. J Cryst Growth, 2011, 316: 172−176.

[18] ZHEN S, DAVIES G J. Observations of the growth morphology of the intermetallic compound Al_3Zr [J]. J Cryst Growth, 1983, 64: 407−410.

[19] SEKERKA R F. Morphological stability [J]. J Cryst Growth, 1968, 3−4: 71−81.

[20] CHERNOV A A. Stability of faceted shapes [J]. J Cryst Growth, 1974, 24−25: 11−31.

[21] JACKSON K A. On the theory of crystal growth: Growth of small crystals using periodic boundary conditions [J]. J Cryst Growth, 1968, 3−4: 507−517.

[22] PAPAPETROU A. Investigations on dendritic growth of crystals [J]. Crystalline Materials, 1935, 92: 89−130. (in German)

[23] ABRAMOV O V. High-intensity ultrasonics: Theory and industrial applications [M]. Amsterdam: Gordon and Breach Science Publishers, 1998.

[24] SANDER J R G, ZEIGER B W, SUSLICK K S. Sonocrystallization and sonofragmentation [J]. Ultrason Sonochem, 2014, 21: 1908−1915.

[25] WANG G, DARGUSCH M S, QIAN M, ESKIN D G, STJOHN D H. The role of ultrasonic treatment in refining the as-cast grain structure during the solidification of an Al−2Cu alloy [J]. J Cryst Growth, 2014, 408: 119−124.

[26] HUNT J D, JACKSON K A. Nucleation of the solid phase by cavitation in an undercooled liquid which expands on freezing [J]. Nature, 1966, 211: 1080−1081.

[27] HAN Y, LI K, WANG J, SHU D, SUN B. Influence of high-intensity ultrasound on grain refining performance of Al−5Ti−1B master alloy on aluminium [J]. Mater Sci Eng A, 2005, 405: 306−312.
[28] FAN Z, WANG Y, XIA M, ARUMUGANATHAR S. Enhanced heterogeneous nucleation in AZ91D alloy by intensive melt shearing [J]. Acta Mater, 2009, 57: 4891−4901.
[29] LI H T, WANG Y, FAN Z. Mechanisms of enhanced heterogeneous nucleation during solidification in binary Al−Mg alloys [J]. Acta Mater, 2012, 60: 1528−1537.
[30] HYDE K B, NORMAN A F, PRANGNELL P B. The effect of cooling rate on the morphology of primary Al_3Sc intermetallic particles in Al−Sc alloys [J]. Acta Mater, 2001, 49: 1327−1337.

超声处理对 Al−0.4Zr 合金中生成的初生 Al_3Zr 金属间化合物的影响

汪 锋[1]，D. ESKIN[1,2], T. CONNOLLEY[3], Jia-wei MI[4]

1. Brunel Centre for Advanced Solidification Technology,
Brunel University London, Uxbridge, London, UB8 3PH, UK;
2. Tomsk State University, Tomsk 634050, Russia;
3. Diamond Light Source Ltd, Harwell Science & Innovation Campus, Didcot, OX11 0DE, UK;
4. School of Engineering, University of Hull, Hull, East Yorkshire, HU6 7RX, UK

摘　要：通过在 Al−0.4Zr 合金凝固过程中外加超声场研究超声处理对 Al_3Zr 金属间化合物形成的影响。超声处理分别采用在凝固过程中的 3 个温度区间：830~790 °C(高于液相线)、790~750 °C(横跨液相线)和 750~710 °C(低于液相线)。超声处理后利用扫描电子显微镜对铸态合金中生成的 Al_3Zr 金属间化合物的尺寸和形貌进行分析观测。结果显示，超声处理后 Al_3Zr 金属间化合物的尺寸显著减小而且形貌也从流星镖状转变成细小片状。讨论 Al_3Zr 金属间化合物超声细化机理。结果表明，超声处理高于液相线时形成的细化效果主要是由于空化气泡激发氧化铝颗粒成为 Al_3Zr 金属间化合物形核质点从而提高形核率；超声处理低于液相线时形成的细化效果主要是由于空化气泡打断生长中的 Al_3Zr 金属间化合物。

关键词：超声处理；铝合金；初生 Al_3Zr 金属间化合物；细化；晶体形貌

(Edited by Xiang-qun LI)